Solvent Quality Dependent Continuum van der Waals Attraction and Phase Behavior for Colloids Bearing Nonuniform Adsorbed Polymer Layers

Michael A. Bevan,* Simon N. Petris, and Derek Y. C. Chan

Particulate Fluids Processing Centre, University of Melbourne, Victoria, 3010, Australia

Received April 1, 2002. In Final Form: July 1, 2002

A liquid−gel transition measured for a polymerically stabilized dispersion as a function of solvent quality and particle volume fraction is compared with theoretical predictions of phase behavior. The experimental liquid−gel transition is interpreted from rheological measurements of 360 nm polystyrene (PS) particles with adsorbed F108 Pluronic (PEO−PPO−PEO) layers in aqueous 0.5 M NaCl as a function of temperature, which controls solvent quality for the adsorbed Pluronic. The measured liquid−gel transition occurs at temperatures when attractive interactions are not expected to occur from either core PS particle van der Waals forces or Pluronic mixing interactions. To consider an alternative temperature dependent attraction, an adhesive sphere (AS) phase diagram is constructed using a theoretical potential that includes the solvent quality dependent continuum van der Waals attraction due to the nonuniform dielectric properties of the adsorbed Pluronic. An impressive correspondence is found between the experimental liquid−gel transition and the theoretical AS percolation threshold with no adjustable parameters using the nonuniform film model. This work indicates conditions when adsorbed polymeric van der Waals interactions are critical for interpreting and predicting solvent quality dependent phase behavior in polymerically stabilized systems.

Introduction

In the "typical" explanation of polymeric stabilization, polymer is adsorbed to colloidal particles, as shown in Figure 1, so that it is thick enough to generate repulsion of sufficient range and magnitude to dominate core particle van der Waals attraction. Similar to the separate treatment of electrostatic and van der Waals interactions in the classic DLVO theory, the "typical" description of polymeric stabilization considers adsorbed polymeric interactions and core particle continuum van der Waals interactions as independent problems. Within this framework, much of the theoretical effort for understanding polymeric stabilization has focused on quantifying interactions between adsorbed polymer layers in terms of their molecular interactions and structures.[1−3]

However, it is not necessarily appropriate to treat polymeric stabilization as an analogue of electrostatic stabilization. Adsorbed polymer consists of a relatively immobile, nonfluid, connected structure with dielectric properties that can be significantly different from both the core colloid and continuous medium properties. In contrast to electrical double layers, adsorbed polymer is generally expected to contribute to the net continuum van der Waals attraction between particles.[4] Adsorbed polymer layers also generate a physical repulsion more analogous to the hard wall interaction between bare colloidal surfaces than the interaction due to a fluid ion distribution. Considering these differences, it is perhaps more accurate to treat polymerically stabilized particles as composite particles consisting of a uniform core and a nonuniform solvated polymeric layer. The core particle and adsorbed polymer together determine the net continuum van der Waals attraction at the composite particle's collision edge, which is defined as the point that the adsorbed polymer density profile vanishes to zero. Within this framework, polymeric stabilization is more generally described in terms of the adsorbed polymer's role of minimizing attraction between particles.[1]

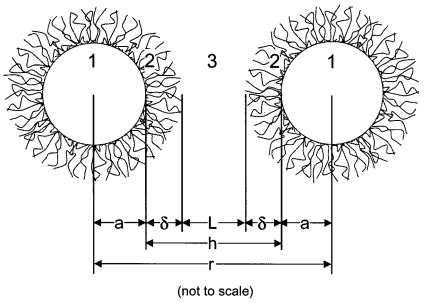

Figure 1. Schematic illustration of relevant separations defined for the interaction of colloidal particles with adsorbed polymer as a function of solvent quality (not to scale).

Although it is somewhat intuitive that adsorbed polymer should contribute to the net van der Waals attraction between polymer coated colloids, the "typical" description of polymeric stabilization is often adequate for understanding dispersion stability. The success of the typical description is due to the fact that highly solvated polymer layers in "good" solvent conditions have dielectric properties that are similar to the medium properties, which results in a minimal van der Waals contribution from the adsorbed polymer. This has been shown by direct measurements of the interaction between polymer coated surfaces in good solvent conditions,[5,6] which have identified

* To whom correspondence should be addressed. E-mail: mabevan@tamu.edu. Current address: Department of Chemical Engineering, Texas A & M University, College Station, TX 77843-3122.

(1) Napper, D. H. *Polymeric Stabilization of Colloidal Dispersions*; Academic Press: New York, 1983.
(2) Fleer, G. J.; Stuart, M. A. C.; Scheutjens, J. M. H. M.; Cosgrove, T.; Vincent, B. *Polymers at Interfaces*; Chapman & Hall: New York, 1993.
(3) Israelachvili, J. N. *Intermolecular and Surface Forces*, 2nd ed.; Academic Press: New York, 1992.
(4) Russel, W. B.; Saville, D. A.; Schowalter, W. R. *Colloidal Dispersions*; Cambridge University Press: New York, 1989.
(5) Bevan, M. A.; Prieve, D. C. *Langmuir* **2000**, *16*, 9274.
(6) Bevan, M. A.; Prieve, D. C. In *Polymers in Particulate Systems: Properties and Applications*; Hackley, V. A., Somasundran, P., Lewis, J. A., Eds.; Marcel Dekker: New York, 2001; Vol. 104.

10.1021/la020308z CCC: $22.00
Published on Web 09/13/2002

a finite but relatively insignificant continuum van der Waals contribution due to the layers. If the goal is to design for polymeric stabilization in guaranteed near "optimal" solvent conditions where layers are primarily composed of solvent, it is reasonable to ignore the adsorbed polymer properties when calculating van der Waals attraction.

In the event that a polymerically stabilized dispersion experiences a change from near optimal solvent conditions, a dimensional collapse and densification of the adsorbed polymer increase the polymeric van der Waals contribution, which is also accompanied by an increased core particle contribution. This is a highly probable situation in practice, given that "solvent quality" for adsorbed polymer (both nonionic and polyelectrolyte) is altered by numerous factors including ionic strength, pH, cosolvents, cosolutes, temperature, and pressure. Adsorbed layers in "poor" solvent conditions become dense in polymer dielectric properties and dissimilar to medium properties, which can result in a significant van der Waals contribution from the adsorbed polymer. In the limit of a total layer collapse to a homogeneous film with bulk polymer properties, an adsorbed polymer layer will contribute its maximum van der Waals attraction. The change in polymeric van der Waals attraction due to diminishing solvent quality may easily be on the order of the thermal energy, kT, and, therefore, be critical for thermodynamic phase transitions including aggregation, gelation, crystallization, and liquid−vapor phase separation. As a result, any application that seeks to exploit colloidal structure via thermodynamic "phase" engineering will certainly have to quantify and manipulate the adsorbed polymer contribution for polymerically stabilized dispersions.

Despite the suggested importance of continuum polymeric van der Waals interactions, this contribution has seen limited theoretical exploration and probably, as a related outcome, has been overlooked in the interpretation of experimental results. A few relevant theories have been developed for the effects of "uniform"[7−10] and "nonuniform" films[11−14] on continuum van der Waals interactions, but predictions using these theories have not been compared with measurements. Numerous experimental investigations have probed solvent quality dependent phase behavior of polymerically stabilized colloids,[15−28] but none of these studies have quantified the role of continuum polymeric van der Waals interactions. Measurements and theories appear to be available for interpreting the role of polymeric van der Waals forces; however, no investigation has yet identified and quantified this effect in phase behavior measurements.

In the present study, solvent quality dependent phase behavior is measured for 360 nm polystyrene (PS) particles with adsorbed F108 Pluronic (PEO−PPO−PEO) layers in aqueous 0.5 M NaCl. In particular, a "liquid−gel" transition is interpreted from previous rheological measurements as a function of temperature and volume fraction.[29] The experimentally observed liquid−gel transition is then compared with an "adhesive sphere" (AS)[30] phase diagram constructed using a theoretical potential that includes the continuum van der Waals attraction due to the solvent quality dependent nonuniform dielectric properties of the adsorbed Pluronic. To our knowledge, this study is unique because (1) the continuum van der Waals attraction between polymer coated colloids is calculated considering both the nonuniform adsorbed polymer and uniform core particle properties as a function of temperature and (2) the resulting attraction is used to make a quantitative comparison of theoretical phase behavior and the experimentally observed transition using no adjustable parameters. This study illustrates the ability to predict macroscopically observable dispersion behavior from fundamental microscopic colloidal interactions.

Theory

Continuum van der Waals Attraction between Colloids Bearing Nonuniform Adsorbed Polymer Layers. To rigorously consider the continuum attraction between polymer coated colloids, as shown in Figure 1, it is necessary to include the *uniform* core particle and *nonuniform* adsorbed polymer layer dielectric properties when computing the net composite particle interaction. The 1975 theory due to Parsegian[13] is one of the few attempts to include nonuniform adsorbed polymer properties for calculating the net van der Waals attraction between a pair of polymer coated colloids. The interaction between polymerically stabilized particles, as shown in Figure 1, can be described generally with a repulsive hard wall term and the attractive composite particle van der Waals term given by Parsegian[13] as

$$E(r) = \begin{cases} \infty, \; 0 < r < 2(a+\delta) \\ -\dfrac{\hbar}{32\pi}\displaystyle\int_0^\infty \mathrm{d}\omega \int_0^{a+\delta} \mathrm{d}r_1 \frac{\mathrm{d}\ln\epsilon(r_1,\omega)}{r_1} \times \\ \qquad \displaystyle\int_0^{a+\delta} \mathrm{d}r_2 \frac{\mathrm{d}\ln\epsilon(r_2,\omega)}{r_2} G(r_1, r_2), \; 2(a+\delta) < r \end{cases} \quad (1)$$

where $G(r)$ is a geometric factor, given by

$$G(r_1,r_2) = \left[\frac{2r_1r_2}{(a+\delta)^2 - (r_1+r_2)^2} + \frac{2r_1r_2}{(a+\delta)^2 - (r_1-r_2)^2} + \ln\left(\frac{(a+\delta)^2 - (r_1+r_2)^2}{(a+\delta)^2 - (r_1-r_2)^2}\right)\right] \quad (2)$$

(7) Vold, M. J. *J. Colloid Sci.* **1961**, *16*, 1.
(8) Langbein, D. *van der Waals Attraction*; Springer-Verlag: Berlin, 1974; Vol. 72.
(9) Mahanty, J.; Ninham, B. W. *Dispersion Forces*; Academic Press: New York, 1976.
(10) Prieve, D. C.; Russel, W. B. *J. Colloid Interface Sci.* **1988**, *125*, 1.
(11) Osmond, D. W. J.; Vincent, B.; Waite, F. A. *J Colloid Interface Sci.* **1973**, *42*, 262.
(12) Vincent, B. *J Colloid Interface Sci.* **1973**, *42*, 270.
(13) Parsegian, V. A. *J. Colloid Interface Sci.* **1975**, *51*, 543.
(14) Kiefer, J. E.; Parsegian, V. A.; Weiss, G. H. *J. Colloid Interface Sci.* **1975**, *51*, 543.
(15) Grant, M. C.; Russel, W. B. *Phys. Rev. E* **1993**, *47*, 2606.
(16) Rouw, P. W.; Vrij, A.; Kruif, C. G. d. *Prog. Colloid Polym. Sci.* **1988**, *76*, 1.
(17) Edwards, J.; Everett, D. H.; OSullivan, T.; Pangalou, I.; Vincent, B. *J. Chem. Soc., Faraday Trans. 1* **1984**, *80*, 2599.
(18) Chen, M.; Russel, W. B. *J. Colloid Interface Sci.* **1991**, *141*, 564.
(19) Jansen, J. W.; Kruif, C. G. d.; Vrij, A. *J. Colloid Interface Sci.* **1986**, *114*, 471.
(20) Jansen, J. W.; Kruif, C. G. d.; Vrij, A. *J. Colloid Interface Sci.* **1986**, *114*, 481.
(21) Jansen, J. W.; Kruif, C. G. d.; Vrij, A. *J. Colloid Interface Sci.* **1986**, *114*, 492.
(22) Jansen, J. W.; Kruif, C. G. d.; Vrij, A. *J. Colloid Interface Sci.* **1986**, *114*, 501.
(23) Vrij, A.; Penders, M. H. G. M.; Rouw, P. W.; Kruif, C. G. d.; Dhont, J. K. G.; Smits, C.; Lekkerkerker, H. N. W. *Faraday Discuss. Chem. Soc.* **1990**, *90*, 31.
(24) Woutersen, A. T. J. M.; Kruif, C. G. d. *J. Chem. Phys.* **1991**, *94*, 5739.
(25) Rouw, P. W.; Kruif, C. G. d. *Phys. Rev. A* **1989**, *39*, 5399.
(26) Everett, D. H.; Stageman, J. F. *Faraday Discuss. Chem. Soc.* **1978**, *65*, 230.
(27) Everett, D. H.; Stageman, J. F. *Colloid Polym. Sci.* **1977**, *255*, 293.
(28) Cowell, C.; Vincent, B. *J. Colloid Interface Sci.* **1982**, *87*, 518.

and the radially dependent dielectric function, $\ln \epsilon(r,\omega)$, describes the composite particle material properties, including the uniform core particle and the nonuniform adsorbed polymer density profile. For uniform core particles of material 1 with nonuniform layers of material 2 in a continuous medium of material 3, as shown in Figure 1, the natural log of the dielectric function in eq 1 is

$$\begin{aligned} \ln \epsilon(r,\omega) = {} & \ln \epsilon_1(\omega)\, H(a-r) && \}\text{core particle} \\ & + \ln \epsilon_2(r,\omega)[H(a+\delta-r) - \\ & \qquad H(a-r)] && \}\text{adlayer} \quad (3) \\ & + \ln \epsilon_3(\omega)\, H(a+\delta-r) && \}\text{medium} \end{aligned}$$

where the polymer layer thickness, δ, is the distance from the core particle surface to the location at which the adsorbed polymer density profile vanishes to zero. The Heaviside step function, H, is used to indicate which material properties contribute to the net interaction as a function of the radial particle coordinate.

Adhesive Sphere Potential and Phase Behavior. The "model" adhesive sphere (AS) potential due to Baxter[30] provides convenient analytical expressions[30−40] and Monte Carlo simulation results[41−44] for predicting solvent quality dependent phase behavior of polymer coated colloids with the "real" potential in eq 1. The AS potential can be written in a form analogous to eq 1 with a repulsive hard wall term, an attractive surface adhesion term, and a term indicating no interaction for separations beyond the range of the surface adhesion as[30]

$$E_{AS}(r) = \lim_{\sigma \to 2(a+\delta)} \begin{cases} \infty, & 0 < r < 2(a+\delta) \\ -\ln\left(\dfrac{\sigma}{12\tau(\sigma - 2(a+\delta))}\right), & 2(a+\delta) < r < \sigma \\ 0, & \sigma < r \end{cases} \quad (4)$$

where τ characterizes the contact adhesion due to an infinitely deep square well with zero width. It is possible to approximate an arbitrary potential, $E(r)$, with the AS potential using the "B_2 device",[31,34] which involves equating the second virial coefficient, B_2, for the AS potential and an arbitrary potential to specify τ as

$$\frac{8(a+\delta)^3}{12\tau} = \frac{8(a+\delta)^3}{3} + \int_0^\infty r^2 \left\{ \exp\left[-\frac{E(r)}{kT}\right] - 1 \right\} dr \quad (5)$$

where the second virial coefficient, B_2, for the AS potential is given by

$$\frac{B_2}{8(a+\delta)^3} = 4 - \tau^{-1} \quad (6)$$

and the second virial coefficient, B_2, for an arbitrary potential is given by

$$B_2 = 12 \int_0^\infty r^2 \left\{ 1 - \exp\left[-\frac{E(r)}{kT}\right] \right\} dr \quad (7)$$

A summary of AS results necessary to construct a phase diagram for comparison with experimental data is given in terms of τ and volume fraction, ϕ, values in Tables 1 and 2. The values for the liquid−vapor coexistence curve in Table 1 were determined by equating chemical potentials and pressures of coexisting phases.[38] Liquid−solid coexistence data in Table 2 were obtained by Marr and Gast using the density functional theory.[40] Values for the percolation threshold are reported in Table 2 for Monte Carlo (MC) simulation results from Lee[42] and analytical results from Chiew and Glandt given by[36]

$$\tau = \frac{19\phi^2 - 2\phi + 1}{12(1-\phi)^2} \quad (8)$$

Table 1. Values of τ and ϕ Used for Liquid−Vapor Coexistence and Spinodal

binodal			spinodal		
τ	ϕ_{gas}	ϕ_{liq}	τ	ϕ_{gas}	ϕ_{liq}
0.0976	0.121		0.0976	0.121	
0.0967	0.0919	0.192	0.0967	0.0933	0.145
0.0950	0.0748	0.238	0.0950	0.0854	0.162
0.0933	0.0639	0.270	0.0933	0.0762	0.174
0.0900	0.0491	0.315	0.0900	0.0635	0.193
0.0833	0.0316	0.376	0.0833	0.0465	0.223
0.0667	0.0126	0.467	0.0667	0.0231	0.271

Table 2. Values of τ and ϕ Used for Percolation, Freezing, and Melting Curves

perc of PY[a]		perc of MC[b]		freezing[c]		melting[c]	
τ	ϕ	τ	ϕ	τ	ϕ	τ	ϕ
0.10	0.095	0.10	0.133	1.5	0.484	1.5	0.661
0.15	0.174	0.15	0.177	1.7	0.487	1.7	0.640
0.20	0.218	0.20	0.210	2	0.488	2	0.613
0.35	0.297	0.35	0.270	3	0.485	3	0.580
0.50	0.345	0.50	0.311	5	0.478	5	0.560
0.70	0.391	0.70	0.352	10	0.470	10	0.546

[a] Reference 36, eq 8. [b] Reference 42. [c] Reference 40.

Results & Discussion

Experimental Temperature Dependent Liquid−Gel Transition. Rheological measurements are shown in Figure 2 for a temperature and particle volume fraction dependent "liquid−gel" transition. These are discussed in detail in a previous manuscript[29] but are summarized here for completeness in the present analysis. To briefly review, Figure 2 reports the shear storage modulus, G', for dispersions of 360 nm polystyrene (PS) particles with adsorbed F108 Pluronic (PEO−PPO−PEO) layers for temperatures of $T = 40-95$ °C and effective particle volume fractions of $\phi_{eff} = 0.1-0.4$. The values of ϕ_{eff} were computed from the core particle volume fraction, ϕ_{core}, and are related to the particle number density, n, by eqs 9 and 10, which use the previously measured temperature dependent Pluronic thickness in eq 11.[6,29] In addition to the temperature scale in degrees Celsius in Figure 2, a nondimensional temperature scale given by eq 12 is shown

(29) Bevan, M. A.; Scales, P. J. *Langmuir* **2002**, *18*, 1474.
(30) Baxter, R. J. *J. Chem. Phys.* **1968**, *49*, 2770.
(31) Regnaut, C.; Ravey, J. C. *J. Chem. Phys.* **1989**, *91*, 1211.
(32) Seaton, N. A.; Glandt, E. D. *J. Chem. Phys.* **1987**, *86*, 4668.
(33) Cummings, P. T.; Perram, J. W.; Smith, E. R. *Mol. Phys.* **1976**, *31*, 535.
(34) Stell, G. *J. Stat. Phys.* **1991**, *63*, 1203.
(35) Chiew, Y. C. *J. Chem. Phys.* **1999**, *110*, 10482.
(36) Chiew, Y. C.; Glandt, E. D. *J. Phys. A* **1983**, *16*, 2599.
(37) Smithline, S. J.; Haymet, A. D. J. *J. Chem. Phys.* **1985**, *83*, 4103.
(38) Barboy *J. Chem. Phys.* **1974**, *61*, 3194.
(39) Coniglio, A.; Angelis, U. D.; Forlani, A.; Lauro, G. *J. Phys. A: Math. Gen.* **1977**, *10*, 219.
(40) Marr, D. W.; Gast, A. P. *J. Chem. Phys.* **1993**, *99*, 2024.
(41) Kranendonk, W. G. T.; Frenkel, D. *Mol. Phys.* **1988**, *64*, 403.
(42) Lee, S. B. *J. Chem. Phys.* **2001**, *114*, 2304.
(43) Seaton, N. A.; Glandt, E. D. *J. Chem. Phys.* **1987**, *87*, 1785.
(44) Seaton, N. A.; Glandt, E. D. *J. Chem. Phys.* **1986**, *84*, 4595.

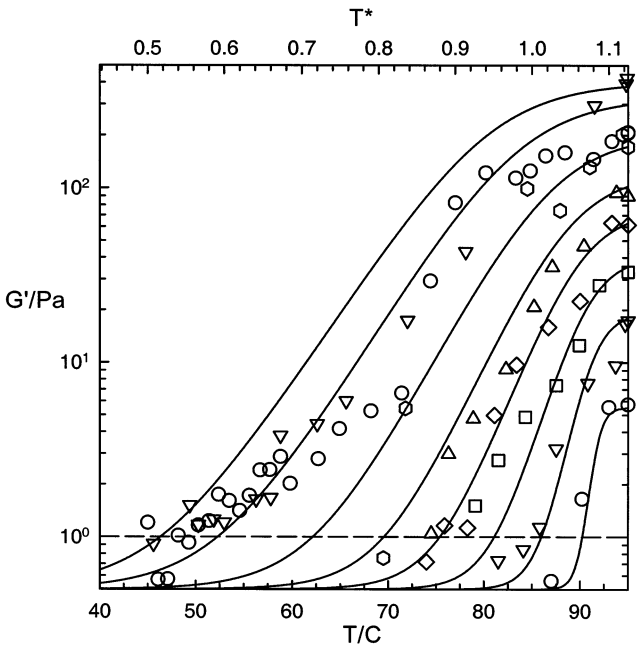

Figure 2. Shear modulus, G' (Pa), as a function of temperature, T (°C), for effective volume fractions (eq 10) at 25 °C of 0.119, 0.162, 0.194, 0.227, 0.2589, 0.302, 0.367, and 0.41. A scale is also shown for the nondimensional temperature, T^* (eq 12). The intersection of the dashed line (- - -) for $G' = 1$ Pa and curve fits (—) (eq 13) indicates values for T_C^* reported in Figure 3 (replotted from ref 29).

to relate the data to critical temperatures for the adsorbed Pluronic. Because the PEO blocks of the triblock Pluronic extend from the PS particle surface[45] and dominate polymeric interactions between layers, the relevant critical temperatures to use in eq 12 are for PEO in 0.5 M NaCl with $\Theta_L = 5$ °C[46] and $\Theta_H = 85$ °C.[47] Empirical curve fits shown in Figure 2 are given by eq 13, which was obtained by fitting each volume fraction data set as a function of T and then fitting the resulting curve fit coefficients as a function of ϕ_{eff} at 25 °C.

$$\phi_{core} = \frac{4}{3}\pi n a_{core}^3 \tag{9}$$

$$\phi_{eff}(T) = \phi_{core}\left[1 + \frac{\delta(T)}{a_{core}}\right]^3 \tag{10}$$

$$\delta^* \equiv \frac{\delta(T^*) - \delta_f}{\delta_0 - \delta_f} = 5.6\ \exp[-\exp(1.6T^* + 0.15)] \tag{11}$$

$$T^* \equiv \frac{T - \Theta_L}{\Theta_H - \Theta_L} \tag{12}$$

$$\frac{G'_{fit}(T,\phi{=}\phi_{eff}(25°C))}{\text{Pa}} = 1 + \frac{m(\phi)}{\left[1 + \exp\left(\frac{b(\phi) - T/\text{K}}{\Delta(\phi)}\right)\right]} \tag{13}$$

$$m(\phi) = \frac{630}{[1 + \exp(3\phi)^{-4.4}]}$$

$$\Delta(\phi) = \frac{5.8}{[1 + \exp(5\phi)^{-3.3}]}$$

$$b(\phi) = 363 - 200\phi^3$$

For each volume fraction measured in Figure 2, the transition from an immeasurable, low value of G' to a finite value is taken to indicate the transition from a "liquid" to a "gel". The continued evolution of G' at temperatures greater than the transition temperatures suggests strengthening of the gel due to increasing particle attraction and possible structural rearrangements. Figure 3 and Table 3 report liquid−gel transition temperatures for each value of ϕ_{eff} when the empirical curve fit in eq 13 has $G'_{fit} = 1$ Pa. The arbitrary functional form of the curve fits, their imperfect representation of the data, and the general criterion for gelation as $G'_{fit} = 1$ Pa indicate significant error ranges for the reported transition temperatures. Although future studies may include more precise measurements and use a better defined criterion for gelation, it will be shown that the liquid−gel transition reported in Figure 3 and Table 3 is sufficient for interpreting the role of continuum polymeric forces.

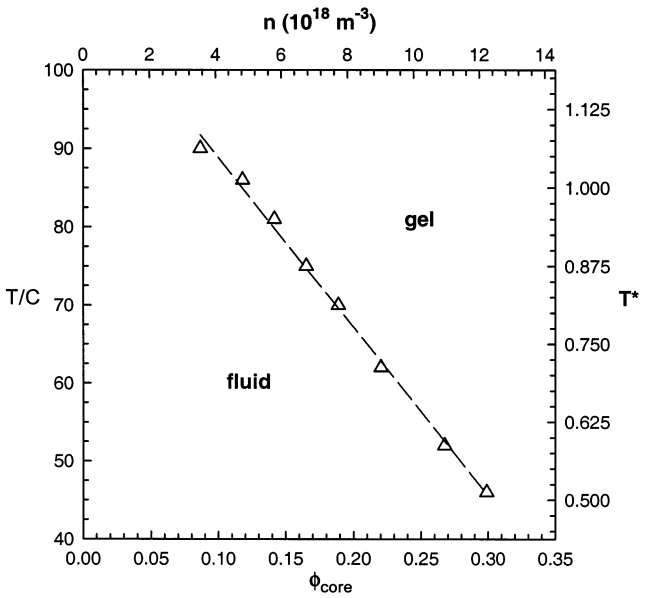

Figure 3. Experimental liquid−gel transition temperatures from Figure 2 as functions of polystyrene core particle volume fractions. A scale is also shown for the polystyrene particle number density (eq 9) and the nondimensional temperature T^* (eq 12) (partially replotted from ref 29).

Table 3. Measured Liquid−Gel Transition and Predicted Percolation Thresholds

$\phi_{core,expt}$	T_{expt}	T_{percPY}	T_{percMC}	$T_{expt} - T_{percPY}$	$T_{expt} - T_{percMC}$
0.0865	90.00	89.20		0.80	
0.118	86.00	84.75	90.64	1.25	−4.64
0.142	81.00	81.76	83.37	−0.76	−2.37
0.165	75.00	78.88	79.05	−3.88	−4.05
0.189	70.00	76.16	75.46	−6.16	−5.46
0.220	62.00	72.72	70.85	−10.72	−8.85
0.267	52.00	67.67	64.64	−15.67	−12.64
0.299	46.00	64.30	60.70	−18.30	−14.70

When considering possible attractive interactions responsible for the observed liquid−gel transition, neither attractive Pluronic mixing interactions nor core PS particle van der Waals interactions are expected for the conditions probed in Figures 2 and 3. A polymeric mixing attraction is expected to occur only for temperatures greater than $T = \Theta_H = 85$ °C, or $T^* = 1$,[47] but the measured liquid−gel transition temperatures are below 85 °C (except one point). With regard to core particle van der Waals forces, the

(45) Li, J.-T.; Caldwell, K. D.; Rapoport, N. *Langmuir* **1994**, *10*, 4475.
(46) Chew, B.; Couper, A. *J. Chem. Soc., Faraday Trans. 1* **1973**, *72*, 382.
(47) Florin, E.; Kjellander, R.; Erikson, J. C. *J. Chem. Soc., Faraday Trans. 1* **1984**, *80*, 2889.

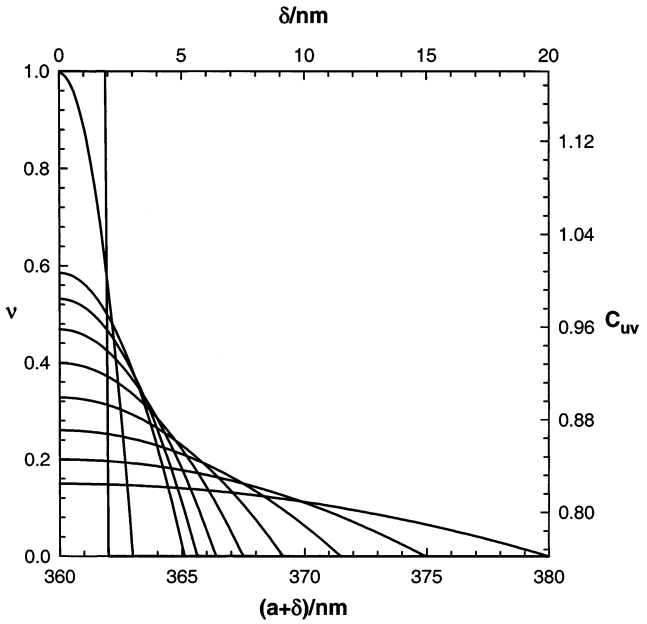

Figure 4. Assumed density profiles for the F108 Pluronic layer on PS as a function of temperature. The adsorbed mass, or area under the density profiles, was measured using reflectometry to be 2 mg/m^2.[58] The temperature dependent thickness (location where the density profile vanishes) was previously measured using total internal reflection microscopy.[5] The value of C_{uv} used to calculate the dielectric function in eq 16 is also shown as a function of concentration (and layer thickness).

saturated F108 Pluronic layers are expected to prevent significant attractive interactions between the 360-nm PS particles at all solvent conditions, which is discussed extensively in previous work.[6,29] Since no other attractive interaction is expected for the experimental conditions probed in Figure 3, the observed liquid−gel phase transition suggests the importance of a continuum van der Waals contribution due to the adsorbed Pluronic. It appears necessary to quantify the Pluronic continuum van der Waals contribution in order to explain the observed liquid−gel transition in Figure 3.

Temperature Dependent Continuum van der Waals Attraction. The potential in eq 1 was originally reported[13] to predict the net van der Waals attraction between particles with nonuniform layers for fixed solvent conditions. To compute temperature dependent attraction between Pluronic coated PS colloids using eq 1, it is necessary to specify the Pluronic temperature dependent density profile and concentration dependent dielectric properties. Measurements have not been made for the temperature dependent density profile of Pluronic adsorbed to PS, but a parabolic "brush" profile can be expected for an adsorbed Pluronic triblock copolymer layer on PS.[2,48−51] Using the temperature dependent Pluronic thickness in eq 11 and a literature adsorbed amount of 2 mg/m^2,[52] a reasonable estimate of the temperature dependent Pluronic density profile, $\nu(r,T)$, is given by eq 14 and shown graphically in Figure 4. This density profile preserves the adsorbed amount of 2 mg/m^2 for all temperatures by varying the Pluronic concentration at the PS particle surface inversely with the layer thickness in eq 11 (Pluronic density assumed to be 1 g/cm^3).

$$\nu(r,T^*) = 0.147\{0.26 + 0.74\exp[-\exp(1.6T^* + 0.15)]\}^{-1}\{1 - [r/\delta(T^*)]^2\} \quad (14)$$

With the temperature dependent density profile in eq 14, now only the concentration dependence of the Pluronic dielectric properties needs to be specified to use the potential in eq 1. Since the Pluronic density profile normal to the PS particle surfaces consists of mostly PEO,[45] the Pluronic dielectric properties are obtained by fitting eq 15 to refractive index data for PEO solutions of varying concentration using the "Cauchy plot" method, described by Hough and White.[53] Figure 5 shows fits to aqueous PEO, PEG, and Pluronic refractive index data for concentrations of $\nu = 0.05-0.5$. The fit results are reported in Table 4 with each fit producing a linear slope of ω_{uv}^{-2} independent of PEO concentration and an intercept C_{uv} that is linearly dependent on PEO concentration. The temperature and radially dependent dielectric properties of the adsorbed Pluronic layer can now be specified in eq 1 using the dielectric function in eq 16 and the density profile in eq 14. Literature values of ω_{uv} and C_{uv} to represent the dielectric properties of PS and water using eq 16 are also reported in Table 3 (with no radial or

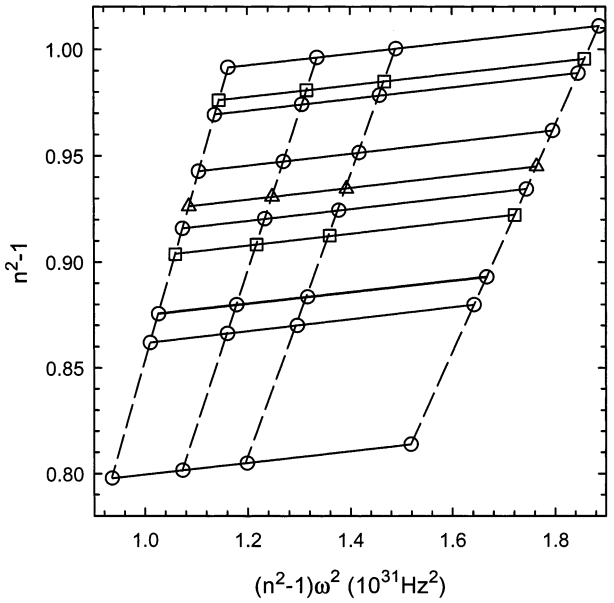

Figure 5. Cauchy plot of $(n^2 - 1)$ plotted against $(n^2 - 1)\omega^2$ for 8000 MW PEO (○) solutions with $\nu = 0.05$, 0.20, 0.26, 0.33, 0.39, 0.45, and 0.50, for 400 MW PEG (□) solutions with $\nu = 0.30$ and 0.47, and for a F108 Pluronic (△) solution with $\nu = 0.35$. The refractive indices were measured at wavelengths of 436, 488, 515, and 550 nm. The solid curves (—) show fits to the data at each PEO concentration, and the dashed curves (- - -) are shown to illustrate the consistency of the data (replotted from ref 29).

Table 4. Dielectric Properties of Materials for van der Waals Calculations

	material	C_{uv}	ω_{uv} (10^{16} rad/s)
polystyrene[a]	1	1.554	1.535
Pluronic (PEO/H_2O)	2	$0.762 + 0.417\nu$	1.900
H_2O[a]	3	0.762	1.992

[a] Reference 54.

(48) Baker, S. M.; Callahan, A.; Smith, G. S.; Toprakcioglu, C.; Vradis, A. A. *Physica B* **1998**, *241−243*, 1041.
(49) Baker, S. M.; Smith, G. S.; Anastassopoulos, D. L.; Toprakcioglu, C.; Vradis, A. A.; Bucknall, D. G. *Macromolecules* **2000**, *33*, 1120.
(50) Ikvov, R.; Butler, P. D.; Satija, S. K.; Fetters, L. J. *Langmuir* **2001**, *17*, 2999.
(51) Karim, A.; Satija, S. K.; Douglas, J. F.; Ankner, J. F.; Fetters, L. J. *Phys. Rev. Lett.* **1994**, *73*, 3407.
(52) Stenkamp, V. S.; Berg, J. C. *Langmuir* **1997**, *13*, 3827.
(53) Hough, D. B.; White, L. R. *Adv. Colloid Interface Sci.* **1980**, *14*, 3.

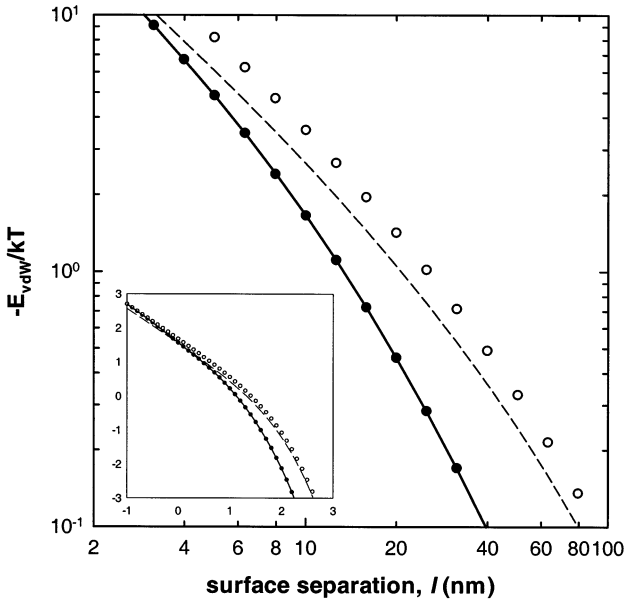

Figure 6. Comparison of retarded and nonretarded van der Waals attractions between bare 360 nm PS particles shown on the positive log scale. The Lifshitz theory and Hamaker geometric correction were used to calculate the retarded (●) and nonretarded attraction (○), as described elsewhere.[55] The dashed curve (- - -) was calculated using eq 1 without material #2. The solid curve (—) is the nonretarded prediction from eq 1 (- - -) multiplied by the correction in eq 17. The inset shows extended log scales.

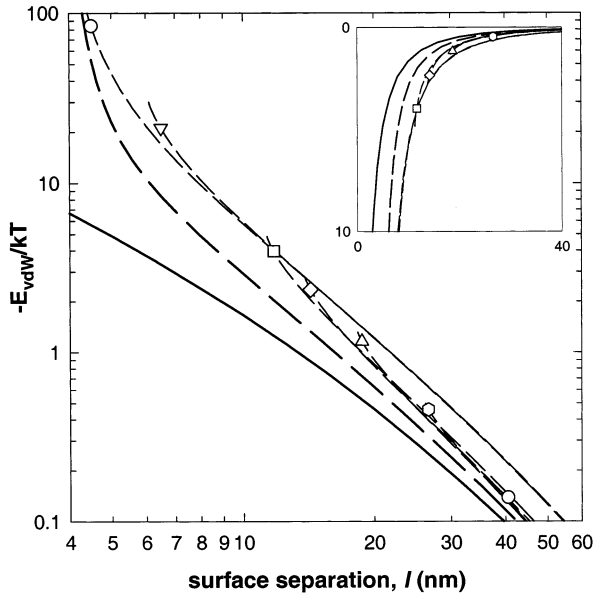

Figure 7. van der Waals attraction between 360-nm PS particles: no adsorbed Pluronic given by solid curve (—), uniform 2-nm Pluronic coating given by long dashes (— — —), and nonuniform coatings given by eq 14 with thicknesses of 2.5, 3, 5.5, 7, 9, 13, and 20 nm given by short dashes (- - -). The inset shows typical van der Waals curves on a typical linear scale.

temperature dependence).[54,55] For polar molecules such as water and PEO that have permanent dipoles, the dielectric constant is also typically included in eq 16; however, the 0.5 M NaCl used in these experiments completely screens this term.

$$n^2(\omega,\nu) = 1 + \frac{C_{uv}(\nu)}{1 - [\omega/\omega_{uv}(\nu)]^2} \tag{15}$$

$$\epsilon_k(r,T^*,\omega) = 1 + \frac{C_{uv,k}[\nu(r,T^*)]}{1 + \{\omega/\omega_{uv,k}[\nu(r,T^*)]\}^2} \tag{16}$$

A possibly significant limitation of the nonuniform film theory in eq 1 is that it does not include the effect of retardation. Retardation weakens attraction between particles at large particle separations because the time for electromagnetic radiation to propagate between molecules and atoms becomes comparable to the lifetime of the fluctuating dipoles that produce van der Waals attraction. It is not obvious whether retardation is significant in the present case because the large surface curvature of the 360 nm PS particles also weakens long-range van der Waals attraction. Since attraction on the order of kT is critical for the liquid−gel transition in Figure 3, it is necessary to address the role of retardation. To quantify the effect of retardation, Figure 6 compares the Lifshitz theory[56,57] with predictions of bare PS interactions calculated using the nonuniform film model in eq 1 with no film (no material #2). The dashed line in Figure 6 shows the nonretarded van der Waals attraction between bare 360 nm PS particles from eq 1 using the PS and water properties in Table 4. The closed and opened circles in Figure 6 show the retarded and nonretarded attractions between bare 360 nm PS particles calculated using the Lifshitz theory and the Hamaker geometric correction, as described in previous work for bare PS interactions[55] (inset shows predictions for 0.1−1000 nm and 10^{-3}−$10^3 kT$).

The difference between the nonuniform film model and the nonretarded Lifshitz result is a maximum of $1.2kT$ for all separations, which shows that eq 1 is quantitatively consistent with the nonretarded Lifshitz theory. The difference between the nonretarded and retarded Lifshitz predictions in Figure 6 is a maximum of $4.7kT$ for the separations of interest in the main figure (and $13.4kT$ for the inset figure). A difference of $4.7kT$ in calculated attraction will dramatically affect predictions of phase behavior, so it is critical to incorporate retardation into eq 1 to interpret the liquid−gel transition in Figure 3. No rigorous method is available to incorporate retardation into inherently nonretarded van der Waals predictions; however, a correction specific to the 360 nm PS particles used in this study is approximated by taking the ratio of eq 1 and the retarded Lifshitz result at all separations with the resulting fitted function (h in nm) given by

$$f(h) = \frac{1.379 - 0.9105h + 3.517h^2 - (2.409 \times 10^{-3})h^3}{1 - 0.4898h + 3.070h^2 + 0.2410h^3 + (3.602 \times 10^{-6})h^4} \tag{17}$$

As shown in Figure 6, multiplying the retardation correction in eq 17 by eq 1 forces the nonuniform film model (solid line) and the retarded Lifshitz theory (solid circles) to predict nearly identical attractions for bare 360 nm PS particles. Retarded van der Waals attraction between 360 nm PS particles with adsorbed Pluronic can now be predicted as a function of temperature using eq 17 in conjunction with eq 1. Figure 7 shows short dashed curves on a positive log scale for van der Waals attraction between 360 nm PS particles with the temperature

(54) Parsegian, V. A.; Weiss, G. H. *J. Colloid Interface Sci.* **1981**, *81*, 285.
(55) Bevan, M. A.; Prieve, D. C. *Langmuir* **1999**, *15*, 7925.
(56) Lifshitz, E. M. *J. Exp. Theor. Phys.* **1955**, *29*, 94.
(57) Dzaloshinskii, I. E.; Lifshitz, E. M.; Pitaerskii, L. P. *Adv. Phys.* **1961**, *10*, 165.
(58) Bevan, M. Ph.D. Dissertation, Carnegie Mellon University, 1999.

dependent Pluronic density profiles shown in Figure 4 (inset shows typical linear scale). Figure 7 also reports Lifshitz predictions for PS particles with uniform 2 nm PEO layers[55] and bare PS particles. Using eq 17 in conjunction with eq 1 appears reasonable from the standpoint that the predictions in Figure 7 are consistent with important theoretical constraints for how coatings modify van der Waals attraction:[13] (1) all curves converge to the PS interaction at long separations, and (2) the nonuniform film model converges to the 2 nm uniform film prediction at short separations.

By including the Pluronic layer density profile and dielectric properties, the nonuniform film model in eq 1 predicts van der Waals attractions of $\sim 1kT$ at 45 °C, $\sim 3kT$ at 70 °C, and $\sim 5kT$ at 85 °C, compared to less than $1kT$ predicted for bare PS particles at temperatures below 90 °C. Since changes in attraction on the order of several kT are critical for the liquid−gel transition in Figure 3, it is essential to include the Pluronic van der Waals contribution. A difficulty with making phase behavior predictions using eq 1 is that a unique potential is predicted for each discrete Pluronic thickness and density profile, as shown by the potentials in Figure 7. To simplify the task of mapping eq 1 onto the adhesive sphere potential in the next section, a single representative curve is reported in eq 18 from a fit to the points shown in Figure 7. While the curve in eq 18 does not exactly fit the nonuniform film model for any given Pluronic density profile, the error due to the fit for all density profiles and separations is less than several tenths of a kT. For reference, the bare 360 nm PS attraction is also accurately given by eq 19 for separations between 0.5 and 100 nm and energies between $100kT$ and $0.01kT$.

$$E_{\mathrm{vdW,PS/PEO}}(h) = \frac{-28.97 + 39.02h - 0.4759h^2 + (1.600 \times 10^{-3})h^3}{1 - 0.9158h + 0.07360h^2 + 0.05770h^3} \quad (18)$$

$$E_{\mathrm{vdW,PS}}(h) = \frac{+489.9 - 8.917h + 0.1221h^2 - (5.236 \times 10^{-4})h^3}{1 + 13.08h + 1.017h^2 + 0.01530h^3} \quad (19)$$

Comparison of Adhesive Sphere Predictions and the Measured Transition. The van der Waals attraction predicted by the nonuniform film model can now be used to construct a phase diagram for comparison with the experimental transition measured in Figure 3. Although it would be desirable to construct a $T-\phi$ phase diagram directly using the nonuniform film potential, generalized analytical predictions have not been derived for arbitrary potentials such as eq 1. To predict phase behavior for the Pluronic coated PS particles used in this study, a suitable approach is to map the nonuniform film potential onto the model adhesive sphere (AS) potential using the "B_2 device".[34] The AS potential is appropriate for predicting equilibrium phase behavior of particles when the range of attraction is less than ~10% of the particle radius,[31] which is the case for potentials in Figure 7. Mapping the nonuniform film potential onto the AS potential involves determination of τ by equating the second virial coefficients, B_2, corresponding to the potentials in eqs 1 and 4. This mapping is depicted graphically in Figure 8 with corresponding values of τ, E_{min}, and B_2 reported as a function of temperature. By using this simple procedure, the $T-\phi$ diagram in Figure 9 was constructed for the Pluronic coated PS particles from the literature τ,ϕ data summarized in Tables 1 and 2 (ϕ_{eff} is used in place of ϕ in the tables). Figure 9 shows the experimental data from Figure 3 as triangles and displays curves for predictions of the spinodal, liquid−vapor coexistence, liquid−solid coexistence, and percolation thresholds (both analytical Percus−Yevick (PY) and Monte Carlo (MC) simulation results).

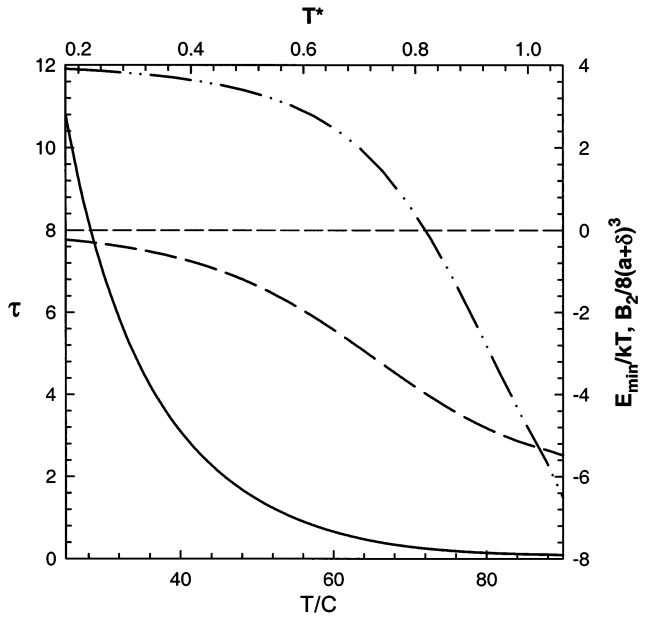

Figure 8. Mapping van der Waals attraction (minimum reported), E_{min}, from eq 1 (— —) onto the AS surface adhesion parameter, τ, in eq 4 (—) by equating second virial coefficients, B_2, in eqs 5−7 (-· · -).

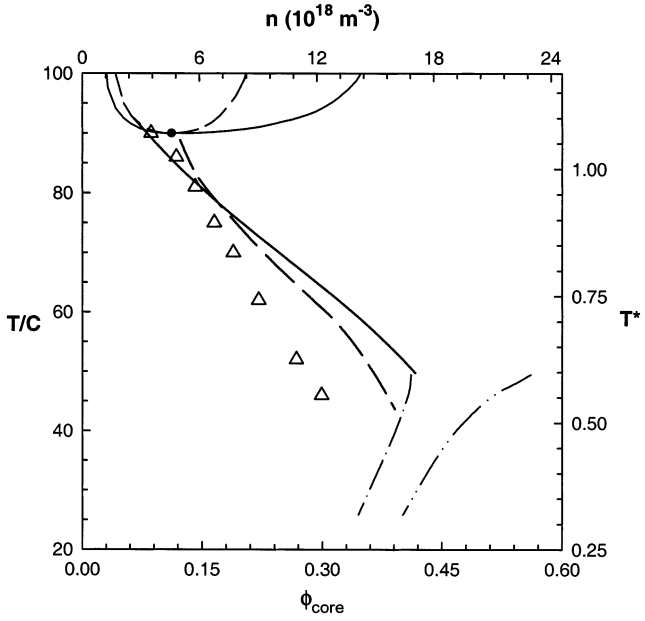

Figure 9. Predicted phase diagram from nonuniform film potential (eqs 1, 14, and 16−18) in conjunction with AS potential (eq 4). Values for liquid−vapor coexistence (—) and spinodal (— — —) reported in Table 1 were determined by equating chemical potentials and pressures of coexisting phases.[38] Liquid−solid coexistence (-· ·-) data in Table 2 from literature results by Marr and Gast were obtained using the density functional theory.[40] Values for the percolation threshold in Table 2 are given by eq 9 from Chiew and Glandt using the Percus−Yevick approximation[36] (—) and also for Monte Carlo simulation results from Lee (— — —).[42]

When comparing the experimental data and AS predictions in Figure 9, there is an obvious correlation between the rheologically measured liquid−gel transition points and the percolation threshold predictions. Table 3 reports values for the liquid−gel data, the percolation predictions, and their differences. The percolation threshold predictions are expected to occur at lower temperatures than those of the measured liquid−gel transition, but the opposite trend is observed in Figure 9. One mechanism that could result in such a discrepancy is a volume fraction dependent compression of the layers due to particle crowding, which has been suggested by literature viscosity measurements.[4] Including this effect as an adjustable parameter in the temperature dependent collapse in eq 11 could easily shift the percolation predictions to coincide with or occur at lower temperatures than those of the measured liquid−gel transition. However, enough uncertainty exists in the liquid−gel data points so that introduction of adjustable parameters is not warranted. Furthermore, refinements of the percolation predictions are not useful because there is no quantitative criterion for comparison with the measured liquid−gel data. Although the percolation threshold and liquid−gel data are certainly expected to be correlated, they are not expected to "agree", since they correspond to different transitions. In any case, the general correspondence observed between the experimental liquid−gel data and the percolation predictions is expected and is quite impressive, since no adjustable parameters were used in constructing Figure 9.

The results in Figure 9 provide more than sufficient evidence that the Pluronic continuum van der Waals contribution is absolutely critical to predicting phase behavior in reasonable correspondence with the experimental liquid−gel data in Figure 3. This is illustrated most simply by noting that if the Pluronic dielectric properties are not considered in eq 1 when constructing Figure 9, no theoretical curves exist below 85 °C. By using a van der Waals potential that includes the measured Pluronic dielectric properties and temperature dependent density profile, it is possible to construct a phase diagram using no adjustable parameters in reasonable agreement with the measured data. The coincidence of the lowest volume fraction data point with the predicted spinodal and the correspondence between the rest of the liquid−gel data points and the percolation predictions suggest that the correct physics are captured by considering the polymeric van der Waals contribution in the AS phase behavior predictions. The general agreement between the data and the predictions in Figure 9 is remarkable, given that this is an initial attempt to consider both polymeric van der Waals forces and predict phase behavior with the AS model for comparison with experimental data using no adjustable parameters.

This work provides the first experimental and theoretical evidence for the important role of adsorbed polymeric van der Waals forces in the phase behavior of polymerically stabilized dispersions. This analysis in combination with previous studies[5,29] can be used to identify the conditions when polymeric van der Waals forces are critical for phase behavior and when they can be ignored. Polymeric van der Waals forces can be important when (1) the polymer layer is thick compared to core particle radius and (2) the average polymer layer dielectric properties are significantly different from the properties of the medium. Although conditions certainly exist when polymeric van der Waals forces can be ignored, as in the "typical" description of polymeric stabilization, this work shows conditions when the polymeric contribution is critical to dispersion phase behavior. Future improvements to this study could involve better measurements of the adsorbed polymer density profile and dielectric properties, as well as better defined measurements of phase transitions. Further refinements to the theories used here could involve a better treatment of retardation, consideration of particle polydispersity, and simulations of phase behavior that directly use an analytical van der Waals potential. Additional experiments to understand the effect of polymeric van der Waals forces in different experimental systems might probe changes in "solvent quality" by altering ionic strength, pH, cosolvents, cosolutes, temperature, and pressure for aqueous polyelectrolytes and solvent based systems.

Conclusions

A rheological liquid−gel transition was measured in PS/Pluronic dispersions for conditions where PS core particle van der Waals and Pluronic mixing attraction were not expected. By using a continuum van der Waals potential that included the nonuniform properties of the adsorbed layer in conjunction with the adhesive sphere model, a predicted phase diagram was constructed in good agreement with the experimental data. In particular, the measured liquid−gel data points displayed a reasonable correspondence with predictions of the percolation threshold and the spinodal. This correspondence illustrates the importance of including the continuum polymeric van der Waals forces for the quantitative prediction of phase behaviors of polymer coated particles as a function of solvent quality. These measurements also indicate the quantitative links between the microscopic interparticle potential and macroscopic phase behavior and rheology in polymerically stabilized dispersions.

Acknowledgment. This work was supported by the Australian Research Council and the Particulate Fluids Processing Centre at The University of Melbourne. Refractive indices of PEO, PEG, and Pluronic solutions were measured by Mr. Mark Kimmel at Carnegie Mellon University.

LA020308Z